Nano Today 68 (2026) 103013

Contents lists available at ScienceDirect

Nano Today

journal homepage: www.elsevier.com/locate/nanotoday

Peptide-specific nanoprobes for matrix-free mass spectrometric imaging of multiplexed proteins and their distributions on cells or tissues

Jiahui Sun, Nan Feng, Si Zhang, Mengchen Wang, Huangxian Ju *

State Key Laboratory of Analytical Chemistry for Life Science, School of Chemistry and Chemical Engineering, Nanjing University, Nanjing 210023, PR China

ARTICLE INFO

Keywords:
Multiplexed proteins imaging
Peptide-specific mass nanoprobes
LDI-MS
Mass spectrometric imaging
Tumor tissues

ABSTRACT

In situ detection of multiplexed proteins is greatly constrained by targeted recognition and operational process. Here we design a one-pot method to synthesize several peptide-specific nanoprobes (NPs) for quickly recognizing the targeted protein molecules, and present a matrix-free laser desorption/ionization mass spectrometric imaging (LDI-MSI) strategy for simple *in situ* imaging of multiplexed proteins on cells or tissues with amplified signals. Unlike conventional citrate-synthesized and post-modified gold nanoparticles, the resulting NPs demonstrate their simple preparation, high resolution and low background with controllable matrix-free and ion-friendly properties. These NPs have been used to conveniently and sensitively detect the relative expression of three specific proteins on four cancer cell lines and efficiently evaluate the suppression of different drugs on these proteins. The proposed MSI method possesses powerful ability to distinctly distinguish different pathological regions of tumor tissues by the change of multiplexed protein distributions, indicating its excellent promise in clinical disease diagnosis and precision medicine.

Introduction

Proteins play important roles in signaling, structural support, and catalysis in living organisms [1], thus their *in situ* and multiplexed detection can provide critical information for a variety of biological and biomedical studies [2]. To provide the spatial information of protein molecules [3], diverse imaging strategies have been developed for *in situ* detection of multiplexed proteins on cells and tissues [4,5]. Among them fluorescence imaging has become general methods for *in situ* visualization of multiplexed proteins [6]. To achieve high-throughput detection of proteins, a cyclic iterative indirect immunofluorescence imaging approach has been proposed through removing the fluorescent signal after each cycle to avoid spectral overlap [7], but this technique suffers from potential loss of epitopes, tissue degradation during repetition, and incomplete inactivation of fluorophores [8]. To overcome these drawbacks, it is highly anticipated to develop simple and rapid strategies for *in situ* detection and high-throughput imaging analysis of multiplexed proteins.

Mass spectrometry (MS) has attractive and evident advantages in the analytical applications of multiplexed proteins due to its high throughput and high sensitivity [9]. It uses *m/z* as its signal, which offers high resolution and can avoid signal crosstalk. Moreover, MS imaging (MSI) enables spatial distribution analysis of various targets synchronously in the same experiment [10]. Especially, matrix-assisted laser desorption/ionization mass spectrometry (MALDI-MS) has been well used in the identification and detection of multiplexed biomarkers due to its convenient preparation of biological tissue samples and salt tolerance [11–13]. To date, MALDI-MS analyses of proteins almost rely either on their enzymatic digestion and detection of peptide segments [14,15], or on the direct *in situ* ionization of proteins in a wide range of *m/z* [16,17]. The former is only applicable to limited proteins with peptide hydrolysis activity, while the latter is limited by the inherently low ionization efficiency. The utilization of nanoprobes and isotopes as mass tags for specific labeling has greatly extended the protein range of MS detection [18–20]. Moreover, nanomaterials with large surface area have shown strong superiority in laser desorption/ionization mass spectrometry (LDI-MS) for the identification and detection of biomarkers over the past decade [21,22]. Some carbon nanomaterials such as single-walled carbon nanohorns possess plentiful inner nanospaces and highly defective horns, which provide high energy transfer efficiency for desorption and ionization of analytes [23]. Of note, nanomaterials instead of traditional organic acid matrices can refine the inherent defects of MALDI-MS, such as strong background noise interference and the lack of reproducibility caused by the heterogeneous

* Corresponding author.
E-mail address: hxju@nju.edu.cn (H. Ju).

https://doi.org/10.1016/j.nantod.2026.103013
Received 4 October 2025; Received in revised form 19 January 2026; Accepted 20 February 2026
Available online 23 February 2026
1748-0132/© 2026 Elsevier Ltd. All rights are reserved, including those for text and data mining, AI training, and similar technologies.

co-crystallization of the analyte and matrix [24]. For instance, Bai et al. achieved the *in situ* mass spectrometric detection and imaging of multiplexed glycans on cells or tissues by bifunctional cleavage probes [25]. However, some issues, such as multi-step modification of lectins and mass tags, steric hindrance caused by lectin itself, and the occurrence of multiple mass peaks from a single mass tag, greatly limit their application. Therefore, it is crucial to develop the mass nanoprobes with the functions of both specific recognition to multiplexed proteins and efficient LDI-MS matrix.

Herein, we designed a one-pot method for convenient synthesis of peptide-specific gold nanoprobes (NPs) through the reduction of $AuCl_4^-$ by the phenolic hydroxyl group of tyrosine in the functional peptides (FPs) [26] and the interaction of NPs with thiol group of cysteine in both the peptides and mass tags (MTs) (Scheme 1a). The FPs on NPs could quickly recognize the targeted proteins on cells or tissues, which led to an LDI-MS strategy for simple *in situ* MSI of multiplexed proteins by using different specific peptides and MTs to synthesize the NPs (Scheme 1b). Compared to conventional citrate-synthesized and post-modified gold nanoparticles, the proposed gold NPs provided controllable matrix-free and ion-friendly properties. Thus, the NPs enabled LDI-MS analysis with low background, while the MTs assured precise distinction of mass peaks. Moreover, the loading of more MTs than FPs led to amplified signals for sensitive detection of the targeted proteins. As a proof of the powerful ability, the designed NPs and the proposed MSI method were applied in simultaneous *in situ* detection of NRP-1, EGFR and $\alpha_v\beta_3$ on cells or tissues and monitoring of the relative expression changes of multiplexed proteins upon external stimuli, which could distinctly distinguish different pathological regions of tumor tissues, demonstrating the potential application in clinical disease diagnosis and precision medicine. The innovative design of the nanoprobes avoids both complex modifications and crosstalk among mass tags, and greatly improves the detection sensitivity for distinctly distinguishing different pathological regions. The simplified operational procedures are also critical for enhancing the clinical practicality of LDI-MSI.

Results and discussion

Verification and performance of NPs with LDI-MS

The NPs specific to NRP-1, EGFR and $\alpha_v\beta_3$ on cells or tissues were synthesized with the mixtures of $AuCl_4^-$ and corresponding FPs (Table S1) and MTs (HS-PEG_8-CH_2CH_2COOH, HS-PEG_2-CH_2CH_2COOH, HS-PEG_4-CH_2CH_2COOH), respectively. The presence of -COOH assured the hydrophilicity of the NPs for improving their accessibility to biological membranes and quickly recognizing the proteins on cells or tissues. After gold nanoparticles absorbed energy under laser irradiation, the Au-S bonds between gold nanoparticles and both FP and MT provided high desorption and ionization efficiency of MTs for MSI. The successful syntheses of the NPs were demonstrated by their LDI mass spectra, which showed the distinct peaks attributing to $[MT1 + Na]^+$, $[2MT2 - H_2 + Na]^+$ and $[MT3 + Na]^+$ at *m/z* 481, 409 and 305, respectively, and a common peak at *m/z* 394, which could be attributed to the presence of $[Au_2]^+$ (Fig. 1a). The peak at *m/z* 425 for NP2 was attributed to $[Au_2 + S - e]^+$.

In order to highlight the advantages of the synthesized NPs for MS analysis, $Au_{15\ nm}$-MT1/FP1 and $Au_{5\ nm}$-MT1/FP1 was synthesized by assembling MT1 and FP1 on citrate-capped both 15-nm and 5-nm gold nanoparticles. Their mass spectra showed the MS peak attributing to $[MT1 + Na]^+$ at *m/z* 481, but more background peaks were observed compared to that of NP1 (Figs. S1 and S2), indicating that citrate-capped gold nanoparticles as matrix were not conducive to the detection of multiplexed MTs. The background peaks resulted from the introduction of salt ions such as Na^+ and citrate ions during the synthesis. The desorption and energy transfer abilities of these gold nanomaterials used as matrices in LDI-MS were assessed with benzyl pyridinium (BP) as a chemical thermometer [27]. Compared to $Au_{15\ nm}$-MT1/FP1 or $Au_{5\ nm}$-MT1/FP1 matrix, the mass specrum of BP using NP1 as matrix exhibited a higher total ion intensity and lower survival yield (Fig. 1b), indicating that NP1 possessed better laser desorption efficiency and efficient ionization capability (Fig. 1c). The photocurrent analysis of these nanomaterials also indicated that NP1 generated the strongest photocurrent signal under ultraviolet laser irradiation (Fig. 1d),

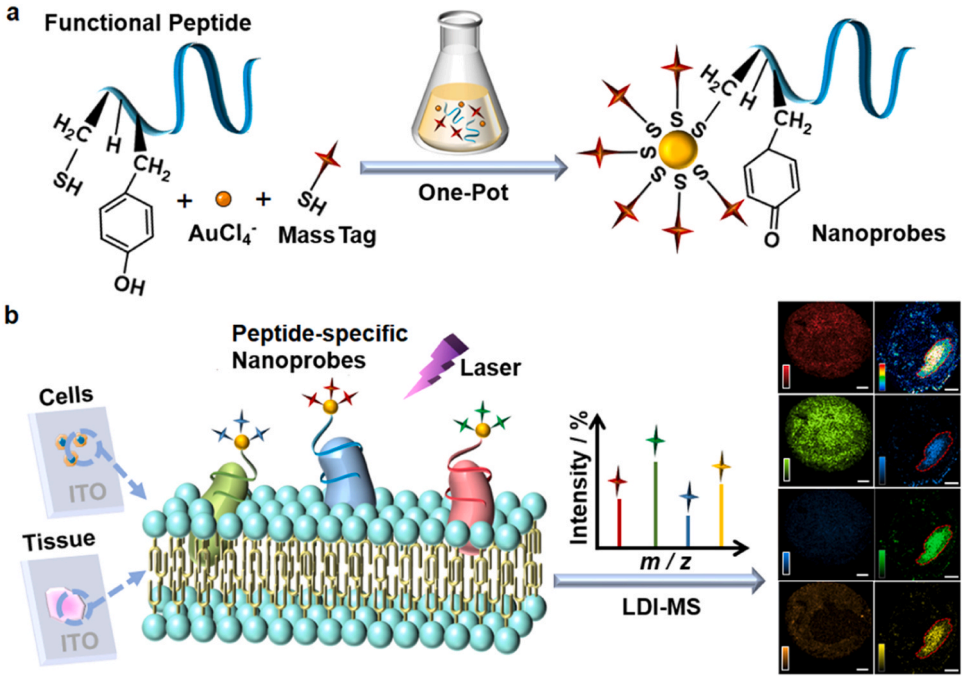

Scheme 1. Schematic illustration. (a) One-pot preparation of peptide-specific nanoprobes. (b) *In situ* LDI-MS detection and imaging of multiplexed proteins on cells or tissues.

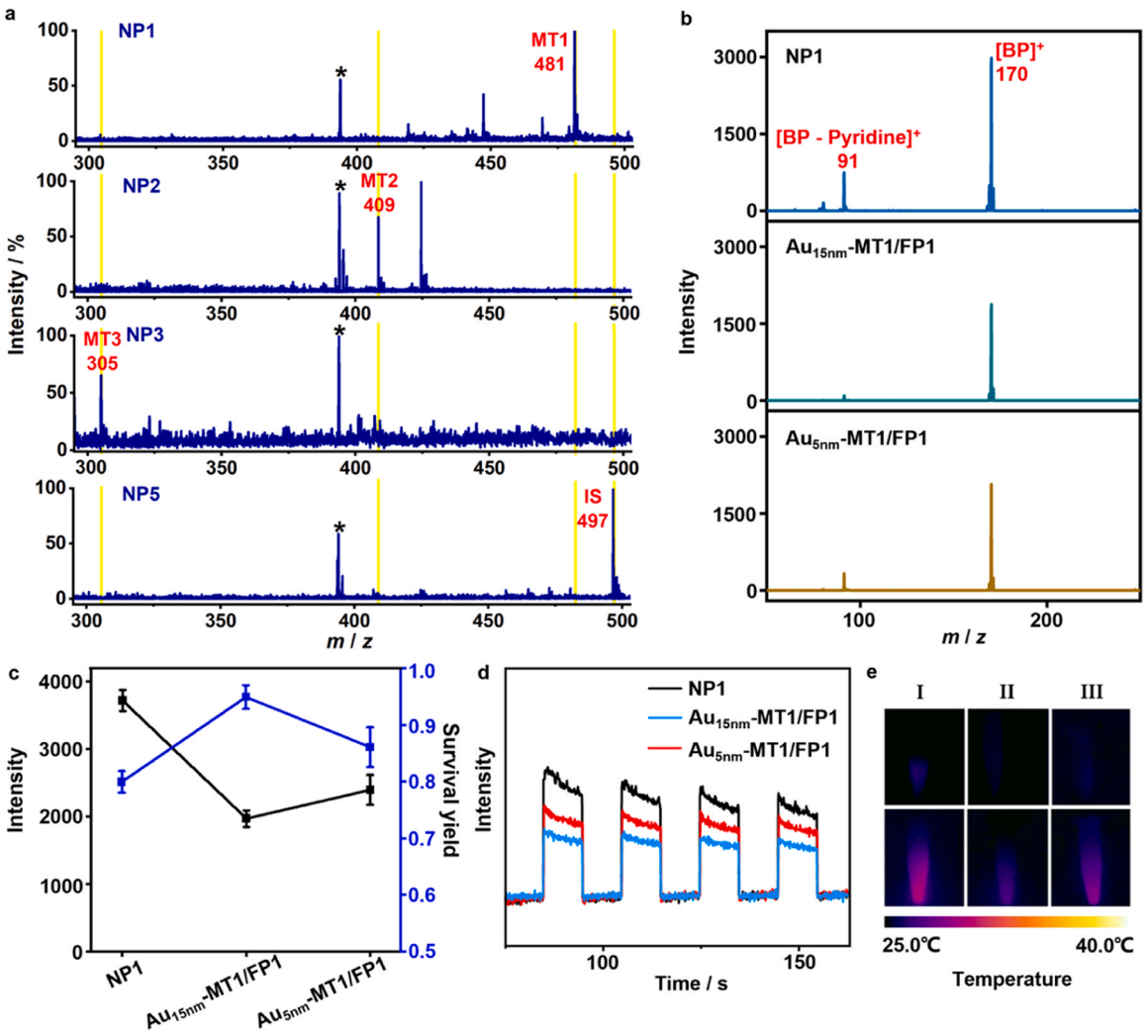

Fig. 1. Verification and performance of NPs with LDI-MS. (a) LDI mass spectra of NP1, NP2, NP3, and NP5 with *m/z* 481 for MT1, 409 for MT2, 305 for MT3 and 497 for IS, respectively. * refers to $[Au_2]^+$. (b) LDI mass spectra of BP ions ($[BP]^+$ at *m/z* 170 and $[BP\text{-pyridine}]^+$ at *m/z* 91) using NP1, $Au_{15\ nm}$-MT1/FP1 and $Au_{5\ nm}$-MT1/FP1 as matrices, respectively. (c) Total intensity of BP ions and survival yield of $[BP]^+$ at *m/z* 170. (d) Photocurrent analysis of NP1, $Au_{15\ nm}$-MT1/FP1 and $Au_{5\ nm}$-MT1/FP1. (e) Infrared thermal images of (I) NP1, (II) $Au_{15\ nm}$-MT1/FP1 and (III) $Au_{5\ nm}$-MT1/FP1 before (top) and after (bottom) laser irradiation.

demonstrating the strong charge transfer capability. The evaluation of photothermal conversion ability further demonstrated the best performance of NP1, which reached a temperature of 30.3 ± 0.2 ℃, slightly higher than 28.7 ± 0.2 ℃ of $Au_{5\ nm}$-MT1/FP1 and 27.6 ± 0.2 ℃ of $Au_{15\ nm}$-MT1/FP1 (Fig. 1e). The higher photothermal conversion ability was beneficial for the desorption of ions [27]. Therefore, NP1 possessed excellent laser desorption and ionization ability due to its specific surface chemical property stabilized by a large amount of FP1 and MT1. In other words, the designed NPs demonstrated their low background for both matrix-free and ion-friendly MS analysis with high sensitivity. In addition, the LDI mass spectrum of NP5 showed the characteristic mass peak of internal standard (IS) at *m/z* 497 $[2IS - H_2 + Na]^+$ (Fig. 1a), which was obviously separated from those of MTs and could serve as IS for quantitative detection of multiplexed proteins.

Optimization and characterization of NPs

To obtain the excellent performance of NPs for MSI of multiplexed proteins, the ratio of FPs to MTs for one-pot synthesis was firstly optimized. With the increasing molar ratio of FP1 to MT1 from 1:10–3:10, the signal (I_{481}/I_{497}) of the obtained NP1 at the same amount increased, and the highest signal occurred at the ratio of 3:10 (Fig. S3), at which the NP1 showed a size of 4.79 ± 0.96 nm (Fig. 2). When the ratio was more than 3:10, more FP1 were loaded on NP1, leading to lower signal. The lower molar ratio of FP1 to MT1 resulted in larger size of NP1 (Fig. 2a-f) due to the presence of less FP1 with the phenolic hydroxyl group for the reduction of Au (III) to Au (0), which slowed down the deposition of Au (0) to obtain larger size. Interestingly, the larger size for more loading of MT1 did not produce strong signal, indicating that the signal was mainly dependent on the thermal conductivity of nanomaterials. The nanomaterials with smaller size possessed lower thermal conductivity [28] for enhancing the ionization efficiency of LDI-MS analysis [29]. Thus, the molar ratio of 3:10 was chose as the optimal ratio for the synthesis of NP1 and other NPs, at which the obtained NPs possessed uniform spherical shape with good mono-dispersity (Fig. 2g and inset in Fig. 2h), and their absorption at 355 nm met the requirement for highly efficient ionization due to the localized

surface plasmon resonance (LSPR) of gold nanoparticles (Fig. 2h). Similarly, NP2, NP3 and NP5 also showed the uniform spherical shape and obvious absorption at 520 nm (Fig. S4), indicating their successful synthesis. In addition, the agarose gel electrophoresis of these NPs showed a single band (Fig. S5), indicating the homogeneous and stable NPs synthesized by the one-pot method.

The presence of MTs and FPs on NPs was further demonstrated with the characteristic FT-IR absorption peaks of NP1 at 3440, 2922, 1386, and 1050 cm^{-1} (Fig. 2i), which were attributed to the stretching

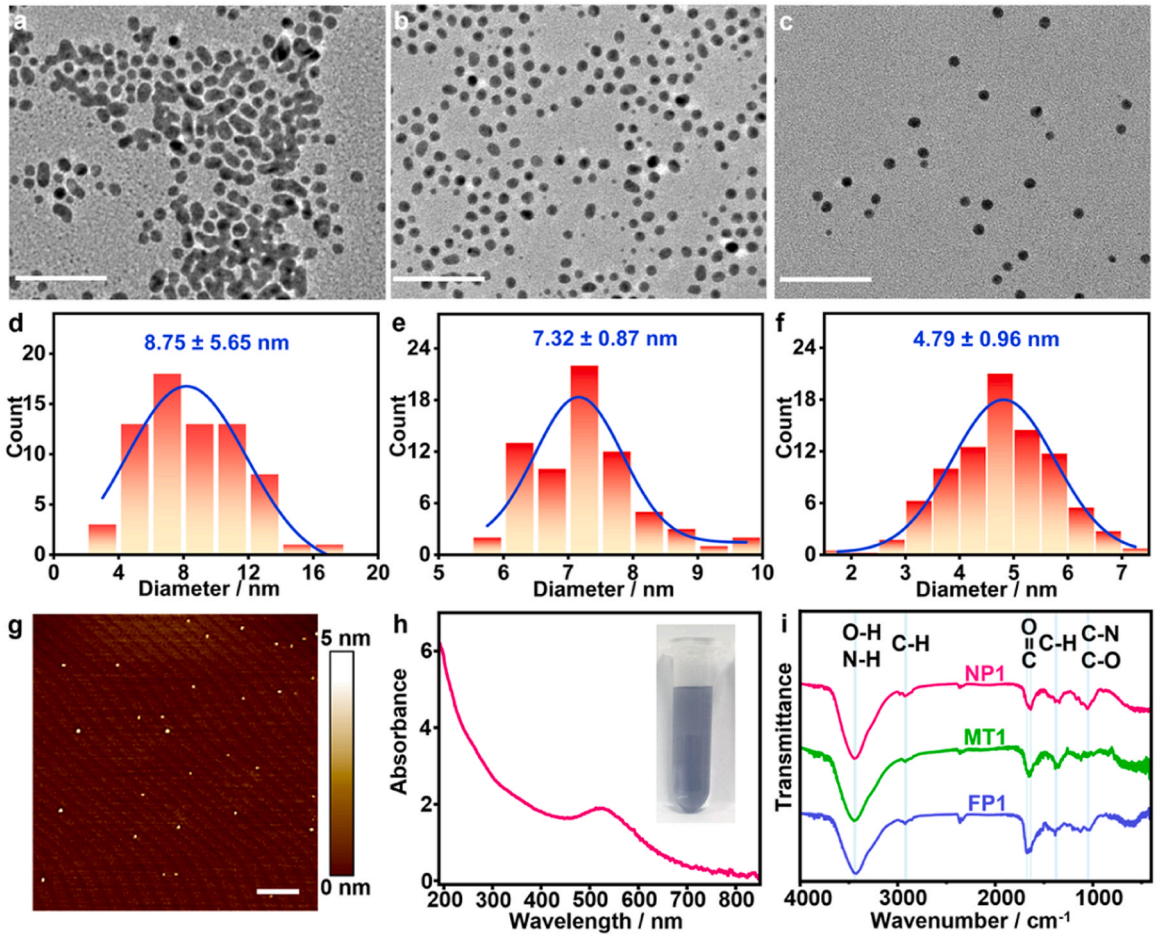

Fig. 2. Optimization and characterization of NPs. (a-c) TEM images and (d-f) size distributions with fitted Gaussian curves of NP1 prepared at FP1 to MT1 ratios of 1:10, 2:10 and 3:10. Scale bars, 50 nm. (g) AFM image of NP1 prepared at 3:10. Scale bar, 0.5 mm. (h) UV-Vis spectrum of NP1 dispersed in PBS. Inset: digital photo. (i) FT-IR spectra of FP1, MT1 and NP1.

vibrations of O-H/N-H, C-H, C-H (CH_3), and C-N/C-O, respectively. The observed redshift of C═O stretching vibration from 1670 cm^{-1} of FP1 to 1636 cm^{-1} of NP1 was attributed to the conversion of the phenolic hydroxyl group into a conjugated carbonyl group, indicating the successful formation of nanoparticles. The conjugation of peptides to the nanoparticles was demonstrated by fluorescence resonance energy transfer (FRET), in which the fluorescence of tyrosine-containing FP1 was quenched by the gold nanoparticles (Fig. S6). The integrity of FPs on NPs was verified using 2,5-dihydroxybenzalacetone (DHB) as an additional matrix to perform MALDI-MS analysis of both free FPs and NPs. The resulting mass spectra of NPs exhibited the characteristic peaks at *m/z* 753, 1708 and 1221, which were close to those of free FPs at *m/z* 784, 1701 and 1220 (Fig. S7), and could be attributed to $[FP1 - S + H]^+$, $[FP2 - S + K]^+$ and $[FP3 + H]^+$, respectively, indicating the presence of complete FPs in NPs for specific recognition of the NPs to targeted proteins. Meanwhile, the effective purification of NP1–3 was achieved after three rounds of centrifugation, which was demonstrated by the MALDI-MS spectra of the supernatants (Fig. S8). The stability and reproducibility of nanoprobes among synthesized batches were also crucial to the reliability and potential applications of the proposed LDI-MSI method. The relative standard deviation (RSD) of the signals (I_{481}/I_{497}) for NP1 at days 1, 7 and 14 was as low as 4.1 % (Fig. S9a), demonstrating excellent stability of the nanoprobes. The RSD of the signal (I_{481}/I_{497}) across five independent batches was 8.0 % (Fig. S9b), indicating good reproducibility of the nanoprobes synthesized by the proposed one-pot method.

In situ visual analysis of multiplexed proteins on cells

Different MTs on NPs possessed different ionization efficiencies, despite their similar molecular structures [30]. To achieve the *in situ* quantitative evaluation of multiplexed proteins on cells with I_{MT}/I_{IS} as the signal, the linear calibration between the signal and the molar ratios of NPs to NP5 as IS was examined under similar environment. The plots the signals vs. the ratios of NP1–3 to NP5 spiked on cells showed good linearity (Fig. 3). The slightly different slopes of these plots implied the difference among the relative ionization efficiencies of MT1- 3. The peaks at *m/z* 449 (Fig. 3c) and 327 were speculated to the cluster ions $[Au_2 + S + Na]^+$ and $[Au_3 + H_2 + Na + K]^{2+}$ (Fig. 3c,e) respectively, which were derived from gold nanoparticles This phenomenon was attributed to uneven drying caused by the direct deposition of nanoparticles on the cells surface, leading to enhanced LSPR of gold nanoparticles during the LDI-MS process [31,32].

To confirm the recognition ability of the NPs to corresponding targeted proteins, HeLa cells as model were firstly seeded in circular holes on ITO slide, which showed uniform distribution across both the central and edged regions of the holes (Fig. S10). Following fixation by 4 % paraformaldehyde solution and incubation with NPs did not show obvious morphological alteration of the cells. The HeLa cells incubated with different NPs and then spiked with NP5 showed individual molecular ion peaks of MTs at *m/z* 481, 305 and 409 and IS at *m/z* 497, respectively (Fig. 4a), while the cells incubated with invalid NPs and then spiked with NP5 showed only the peak of IS (Fig. S11), indicating the specificity of these protein NPs without nonspecific adsorption.

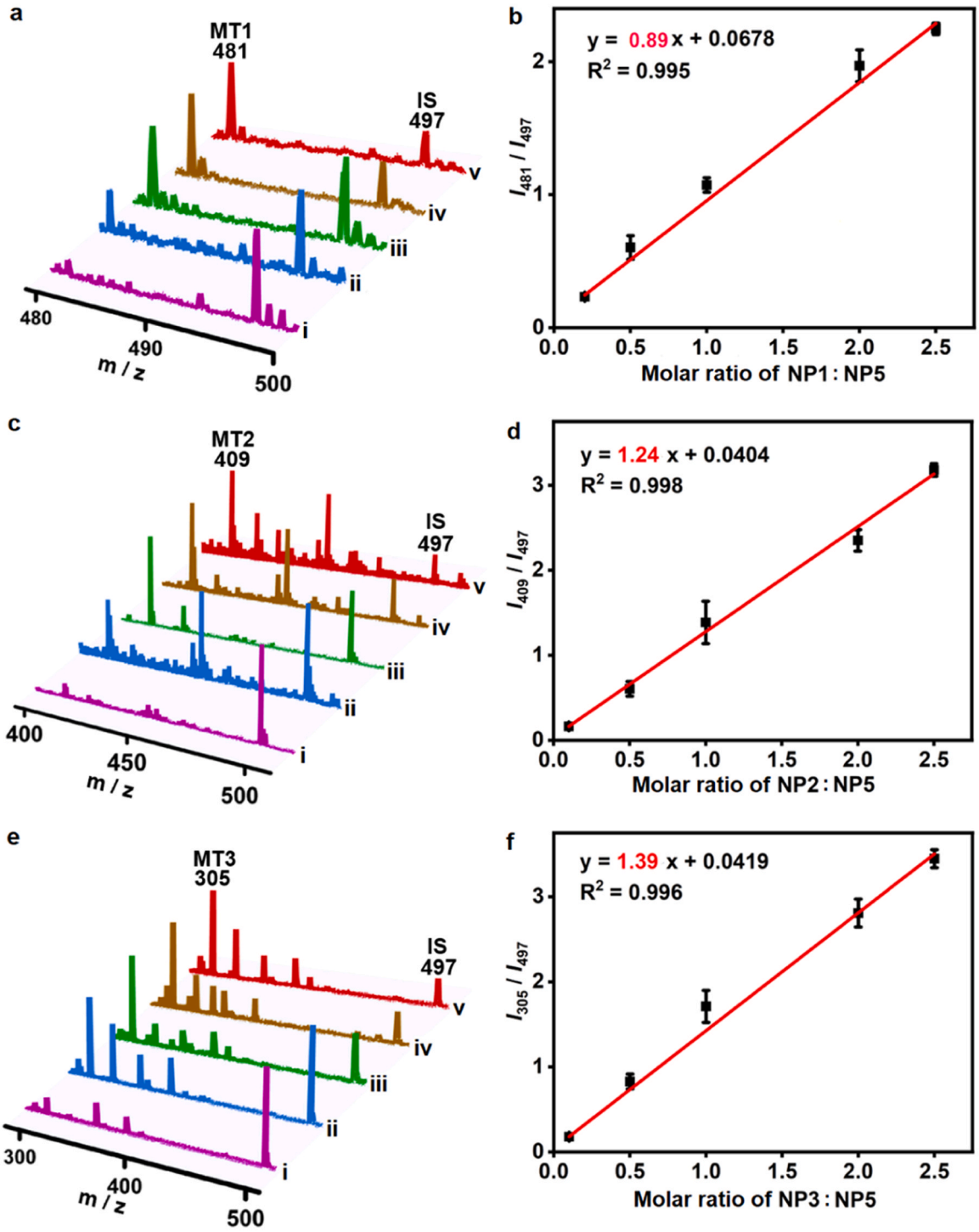

Fig. 3. Linear calibration between signal and molar ratio of NP1–3 to NP5. (a, c, e) LDI mass spectra of NP1 mixed with NP5 at molar ratios of 2:10, 5:10, 10:10, 10:5 and 10:4 for (i)-(v) in (a), NP2 (c) and NP3 (e) mixed with NP5 at molar ratios of 1:10, 5:10, 10:10, 10:5 and 10:4 for (i)-(v). (b, d, f) Plots of corresponding relative intensity vs molar ratio of NP1–3 to NP5.

For detecting multiplexed proteins on HeLa cells, the incubation time with the mixture of NP1–3 was optimized to be 25 min (Fig. S12), indicating a quick recognition process of the FPs to the proteins on fixed cells. Moreover, the LDI mass spectra showed distinct resolution of different MTs on the cells and good repeatability (Figs. 4b and S13). The latter was further demonstrated by the MS images of MTs and IS from three independent parallel experiments, which showed good signal stability and repeated distribution of the HeLa, MCF-7, A549 and 4T1 cells (Figs. S14-S17). These advantages arose from simple detection process and the absence of additional matrix, thereby reducing signal variation from heterogeneous crystallization.

Based on the linear calibration between the peak intensity ratios of MTs to IS and the amounts of NPs along with the slightly different slopes (Fig. 3), the relative quantities of three specific proteins on cell surface could be obtained using the expression of NRP-1 on HeLa cells as 1. The expression of EGFR was approximately 3-fold higher than that of NRP-1, while the expression of NRP-1 was about 6.5-fold higher than that of $\alpha_v\beta_3$ on HeLa cells (Fig. 4c). Meanwhile, HeLa cells exhibited higher

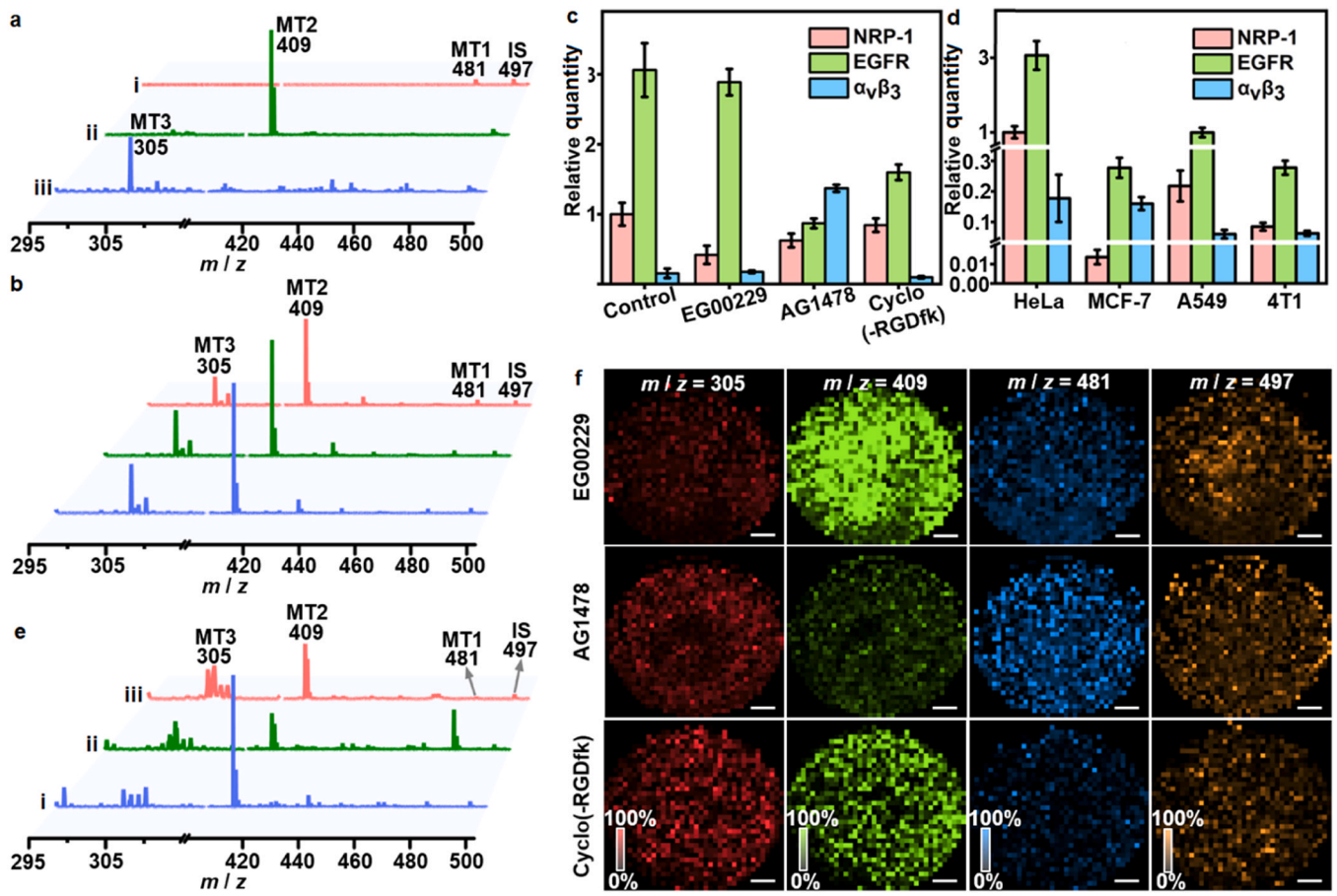

Fig. 4. *In situ* visual analysis of multiplexed proteins on cells. LDI mass spectra of HeLa cells after incubation with (a) NP1 (i), NP2 (ii), and NP3 (iii) and then adding NP5 on cell surface, and (b) the mixture of NP1–3 in three parallel experiments. (c) Relative quantities of three specific proteins on HeLa cells before and after stimuli with different inhibitors. (d) Comparison among the relative quantities of multiplexed proteins on four types of cancer cells. (e) LDI mass spectra of HeLa cells after stimulated with protein inhibitors (i) EG00229, (ii) AG1478 and (iii) Cyclo(-RGDfk), incubated with the mixture of NP1–3 and spiked with NP5 on cell surface. (f) *In situ* MS images of HeLa cells after treated as (e). Scale bars: 0.5 mm. The expression of NRP-1 on HeLa cells is considered as 1. MT1, MT2 and MT3 denote the signal for $\alpha_v\beta_3$, EGFR, and NRP-1, respectively.

EGFR expression level than A549 cells, which was also higher than the comparable levels on MCF-7 and 4T1 cells (Fig. 4d). MCF-7 cells showed significantly lower expression of NRP-1 than other cells, which was consistent with previous reports [33–36] and the results of conventional immunofluorescent testing on four types of cancer cells (Figs. S18-S20), indicating the reliability of the present method.

To demonstrate the practical application of the proposed method in *in situ* quantitative evaluation of multiplexed proteins, HeLa cells were treated with specific protein inhibitors such as EG00229 for NRP-1, AG1478 for EGFR and Cyclo(-RGDfk) for $\alpha_v\beta_3$, which resulted in obviously different mass spectra and MS images (Fig. 4e,f), revealing distinct protein expression alterations upon different inhibitor stimuli. Statistical analysis showed significant differences in protein expressions compared to the control group (Fig. 4c), which were in good agreements with the functions of these inhibitors. Surprisingly, when EGFR expression significantly decreased and NRP-1 expression slightly decreased after treating HeLa cells with AG1478, $\alpha_v\beta_3$ expression showed an increase by 8.9 folds compared to the control group, indicating different intrinsic interactions between protein and the inhibitors. Similar experimental results were also observed by immunofluorescence testing and by flow cytometry, confirming the effectiveness of this method (Figs. S21 and S22). Therefore, the NPs provided a sensitive and specific tool for monitoring the relative expression of multiplexed proteins.

Universality of proposed MSI method and NPs

The simple operation coupled with high resolution and sensitivity allowed this method to be extended to the detection of diverse targeted proteins. For example, NP4 targeting PD-L1, related to the mechanisms for tumor immune evasion [37], was synthesized with FP4 and MT4 (Fig. S23) for the detection of PD-L1 expression on 4T1 cells and *in situ* monitoring of its changes upon different drug treatments. After 4T1 cells were incubated with NP4, a specific peak was observed at *m/z* 349 $[MT4 + Na]^+$, which was also distinguished from the IS at *m/z* 497 (Fig. 5a). Different drug treatments of 4T1 cells led to the difference of mass spectra and MS images (Fig. 5a, b). Statistical analysis indicated that untreated 4T1 cells exhibited high expression of PD-L1 (Fig. 5c), while its relative quantity significantly decreased on dinaciclib group and slightly change foretinib group, demonstrating that dinaciclib treatment led to dramatically reduced PD-L1 expression, and the inhibitory effect of foretinib on PD-L1 expression was weaker, which was consistent with previous report [38], confirming the reliability and expandability of this method. In addition, doxorubicin treatment led to the 39.6 % reduction of PD-L1 expression on 4T1 cells. Therefore, the present protocol provided a universal tool for efficacy evaluation of drugs.

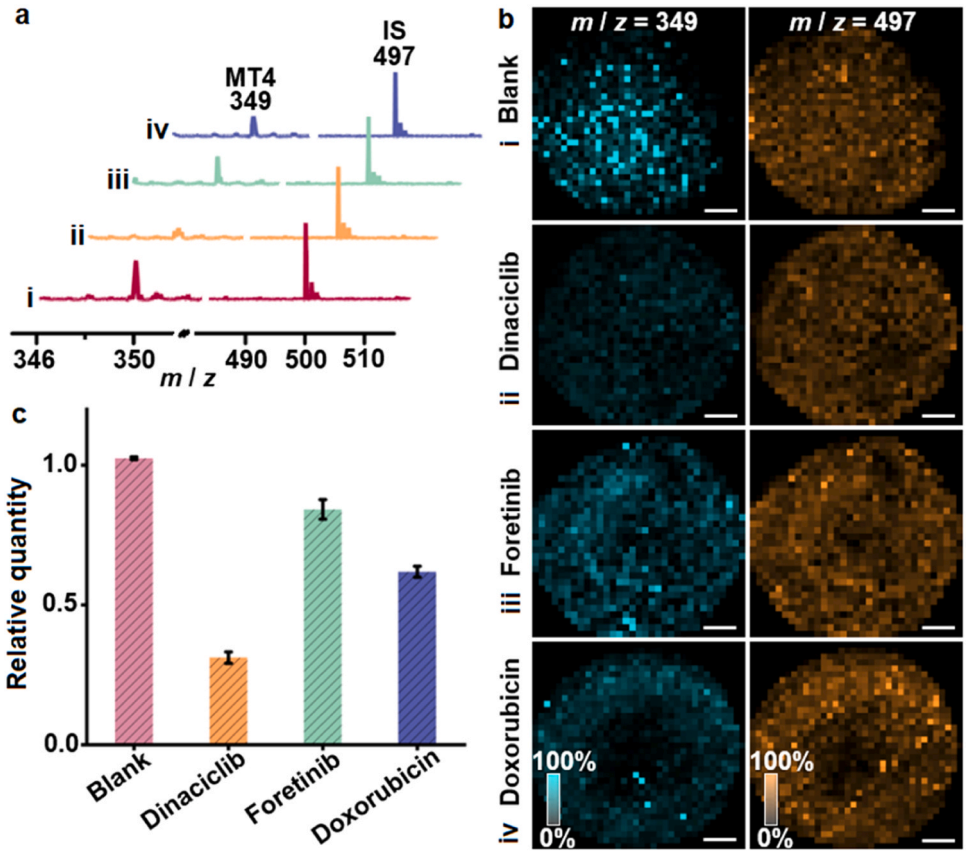

Fig. 5. *In situ* monitoring of PD-L1 expression upon different drug treatments on 4T1 cells. (a) Mass spectra of (i) blank-, (ii) dinaciclib-, (iii) foretinib- and (iv) doxorubicin-stimulated 4T1 cells after incubation with NP4 and then adding NP5 on cell surface. (b) MS images at *m/z* 349 and 497 corresponding to (a). Scale bars: 0.5 mm. (c) Relative quantities of PD-L1 on 4T1 cells after drug stimuli, which are normalized with PD-L1 expression on blank group.

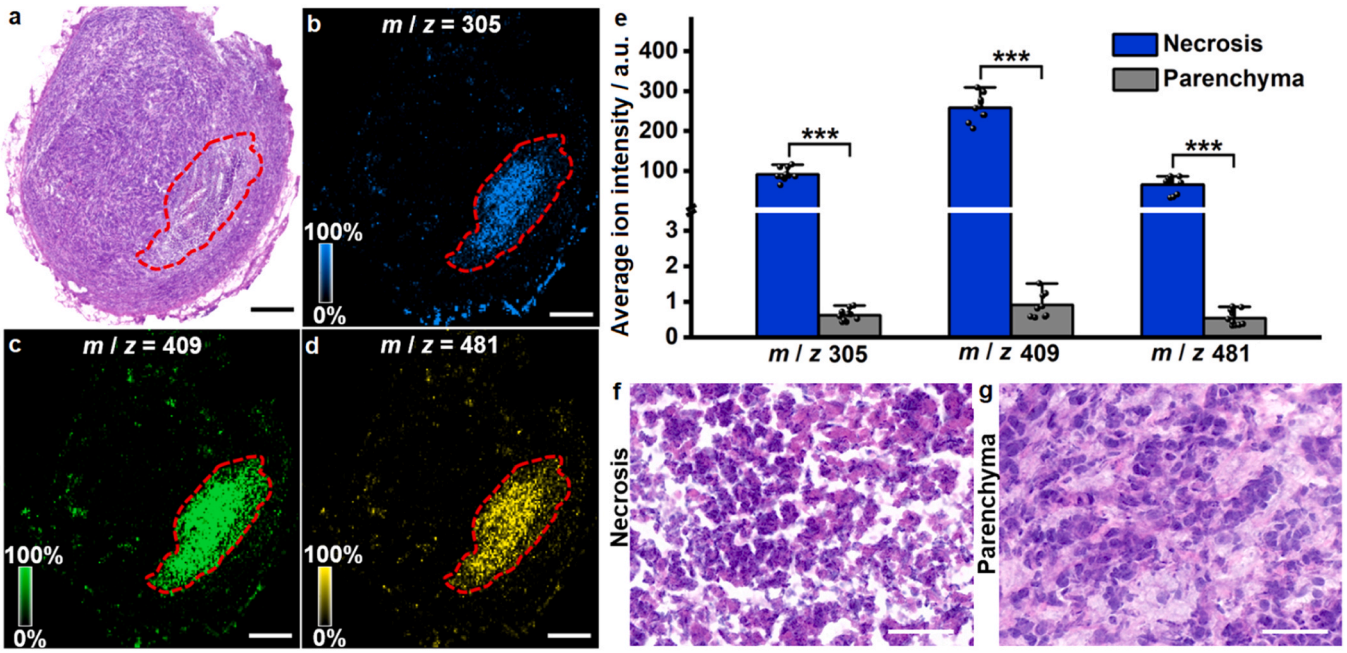

Fig. 6. *In situ* visualization of multiplexed proteins on tumor tissues. (a) Tumor tissue section after H&E staining, which is divided into necrotic and parenchymal regions inside and outside red dash line. Scale bars: 0.5 mm. (b-d) MS images of MT3 for NRP-1 (b), MT2 for EGFR (c) and MT1 for $\alpha_v\beta_3$ (d). Scale bars: 0.5 mm. (e) Average ion intensities of three MTs corresponding to the levels of three proteins in necrotic and parenchymal regions ($n = 10$). ***, $P < 0.001$. (f, g) Enlarged views of H&E stained tissue inside (f) and outside (g) red dashed line. Scale bars: 50 μm.

In situ visualization of multiplexed proteins and their distributions on tumor tissues

Considering the widespread variations of protein expression in biological samples and various diseases, the spatial distribution of multiplexed proteins within tumor tissues is very important in clinic medicine. The applicability of the designed NPs and MSI method was further validated on tissue section of 4T1-bearing mouse subcutaneous tumor, which was divided into necrotic and parenchymal regions with hematoxylin and eosin (H&E) staining (Fig. 6a). After this section was treated with the mixture of NP1–3, its LDI mass spectrum showed the molecule ion peaks of respective MTs (Fig. S24), while all MS images corresponding to MTs showed significantly different information related to these regions (Fig. 6b-d). In necrotic region all of three targeted proteins, NRP-1, EGFR and $\alpha_v\beta_3$, showed much higher levels than those in parenchymal region (Fig. 6e) along with nuclear pyknosis and karyorrhexis, consistent with the morphological hallmarks of necrosis (Fig. 6f), which was completely different from the tumor cell arrangement in nests with prominent nucleoli in parenchymal region (Fig. 6g). The high levels of targeted proteins detected in necrotic region was in agreement with previous reports [39–41], which was possibily attributed to membrane disruption [42] or protein accumulation [43], further validating the feasibility of this strategy.

Given the commonality of tumor heterogeneity, this proposed strategy was also applied to obtain the spatial distribution of three proteins on tumor tissue section from another 4T1-bearing mouse, which was divided into angiogenic, cancerous and epithelial regions with H&E staining (Fig. S25a). These regions could be distinctly distinguished with both the MSI images of different MTs after the section was simply treated with the mixture of NP1–3 targeting three proteins (Figs. S25b-d), and the magnified histological H&E staining images (Fig. S25e). NRP-1, EGFR and $\alpha_v\beta_3$ were highly expressed in the angiogenic region due to the numerous blood vessels compared to the cancerous region, as reported previously [44–46]. Two parts of the cancerous region showed similar MSI images. The epithelial region showed negligible expression of these proteins (Fig. S25f). Therefore, MS images of MTs provided deep insight into differences in protein relative expression and distributions across pathological states and tumor microregions, holding the promise for clinical applications. Compared to the probe-based MSI methods for different types of targets (Table S2), the proposed method showed the advantages of simple synthesis, low time consumption and flexible applications.

Conclusion

This study designed a simple one-pot method to conveniently synthesize peptide-specific NPs containing MTs for quick and specific recognition to targeted proteins, which led to a simple and powerful method for *in situ* MS imaging of multiplexed proteins on cells or tissues. These NPs demonstrated their matrix-free and ion-friendly properties along with good mono-dispersity, and showed low background for multiplexed LDI-MS analysis with separated mass peaks and amplified signals. Moreover, the optimized NPs had low thermal conductivity for improving the ionization efficiency of MTs. Using another NP as internal standard, the relative quantitative detection of multiplexed proteins expressed on different cells was achieved with good reliability, which could be used for visually assessing the effects of various protein inhibitors or drugs on cells, and obtaining the spatial distribution of multiplexed proteins on tissues to accurately distinguish different pathological regions. This innovative method provided a flexible and versatile tool for sensitive and specific monitoring of multiplexed protein expressions, and could be utilized for direct LDI-MS detection and MSI of different targets to meet the demands in biomedicine.

CRediT authorship contribution statement

Mengchen Wang: Software, Formal analysis. **Nan Feng:** Supervision, Formal analysis, Conceptualization. **Si Zhang:** Investigation, Formal analysis. **Jiahui Sun:** Writing – original draft, Validation, Formal analysis, Data curation, Conceptualization. **Huangxian Ju:** Writing – review & editing, Supervision, Methodology, Funding acquisition.

Declaration of Competing Interest

The authors declare that there is no conflict of interest.

Acknowledgements

We gratefully acknowledge the financial supports from the National Natural Science Foundation of China (21890741) and Frontier Technology Research and Development Program of Jiangsu Province (BF2024055).

Supporting information

Supplementary data associated with this article can be found in the online version at https://doi.org/10.1016/j.nantod.

Appendix A. Supporting information

Supplementary data associated with this article can be found in the online version at doi:10.1016/j.nantod.2026.103013.

Data Availability

No data was used for the research described in the article. The data that support the findings of this study are available from the corresponding author upon reasonable request.

References

[1] B.Q. Lin, T. Tian, Y.Z. Lu, D. Liu, M.J. Huang, L. Zhu, Z. Zhu, Y.L. Song, C.Y. Yang, Angew. Chem. Int. Ed. 60 (2021) 7582–7586.
[2] Z.Y. Liao, L. Han, Q.J. Li, L.Y. Li, Y. Liu, Y. Song, W.H. Tan, E.Q. Song, Adv. Funct. Mater. 31 (2021) 2009937.
[3] P.F. Zhang, G.Z. Ma, W. Dong, Z.J. Wan, S.P. Wang, N.J. Tao, Nat. Methods 17 (2020) 1010–1017.
[4] Y.Z. Zhang, Z.Y. Wang, L. Wu, S.F. Zong, B.F. Yun, Y.P. Cui, Small 14 (2018) 1704433.
[5] Y.C. Ou, X.N. Wen, C.A. Johnson, D. Shae, O.D. Ayala, J.A. Webb, E.C. Lin, R. C. DeLapp, K.L. Boyd, A. Richmond, A. Mahadevan-Jansen, M. Rafat, J.T. Wilson, J.M. Balko, M.N. Tantawy, A.E. Vilgelm, R. Bardhan, ACS Nano 14 (2019) 651–663.
[6] Y. Wang, X.Y. Liu, Y.T. Zeng, S.K. Saka, W.X. Xie, I. Goldaracena, R.E. Kohman, P. Yin, G.M. Church, Nucleic Acids Res 52 (2024) e71.
[7] A.J. Radtke, E. Kandov, B. Lowekamp, E. Speranza, C.J. Chu, A. Gola, N. Thakur, R. Shih, L. Yao, Z.R. Yaniv, R.T. Beuschel, J. Kabat, J. Croteau, J. Davis, J. M. Hernandez, R.N. Germain, Proc. Natl. Acad. Sci. U. S. A. 117 (2020) 33455–33465.
[8] J.W. Hickey, E.K. Neumann, A.J. Radtke, J.M. Camarillo, R.T. Beuschel, A. Albanese, E. McDonough, J. Hatler, A.E. Wiblin, J. Fisher, J. Croteau, E.C. Small, A. Sood, R.M. Caprioli, R.M. Angelo, G.P. Nolan, K. Chung, S.M. Hewitt, R. N. Germain, J.M. Spraggins, E. Lundberg, M.P. Snyder, N.L. Kelleher, S.K. Saka, Nat. Methods 19 (2021) 284–295.
[9] R. Aebersold, M. Mann, Nature 537 (2016) 347–355.
[10] Y.R. Xie, D.C. Castro, S.S. Rubakhin, T.J. Trinklein, J.V. Sweedler, F. Lam, Nat. Methods 21 (2024) 521–530.
[11] A. Ly, A. Buck, B. Balluff, N. Sun, K. Gorzolka, A. Feuchtinger, K.-P. Janssen, P.J. K. Kuppen, C.J.H. van de Velde, G. Weirich, F. Erlmeier, R. Langer, M. Aubele, H. Zitzelsberger, L. McDonnell, M. Aichler, A. Walch, Nat. Protoc. 11 (2016) 1428–1443.
[12] J.J. Hu, F. Liu, H.X. Ju, Angew. Chem. Int. Ed. 55 (2016) 6667–6670.
[13] N. Feng, Y.R. Li, J.H. Sun, H.Q. Wang, Q.L. Ma, J.X. Guo, H.X. Ju, Nano Today 50 (2023) 101889.
[14] J.C. McMillen, D.B. Gutierrez, A.M. Judd, J.M. Spraggins, R.M. Caprioli, J. Am. Soc. Mass Spectrom. 32 (2021) 2583–2591.

[15] P.D. Piehowski, Y. Zhu, L.M. Bramer, K.G. Stratton, R. Zhao, D.J. Orton, R. J. Moore, J. Yuan, H.D. Mitchell, Y.Q. Gao, B.M. Webb-Robertson, S.K. Dey, R. T. Kelly, K.E. Burnum-Johnson, Nat. Commun. 11 (2020) 8.
[16] G. Stübiger, M.D. Nairn, T.K. Abban, M.E. Openshaw, L. Mancera, B. Herzig, M. Wuczkowski, D. Senfter, R.M. Mader, Anal. Chem. 90 (2018) 13178–13182.
[17] R. Wu, L. Qin, L.L. Chen, R. Ma, D.F. Chen, H.Q. Liu, H.L. Xu, H. Guo, Y.J. Zhou, X. D. Wang, Chem. Commun. 57 (2021) 10707–10710.
[18] S.T. Xu, W. Ma, Y. Bai, H.W. Liu, J. Am. Chem. Soc. 141 (2019) 72–75.
[19] S.T. Xu, M.X. Liu, J. Feng, G.T. Yan, Y. Bai, H.W. Liu, Chem. Sci. 12 (2021) 4916–4924.
[20] M. Ribéraud, E. Porret, A. Pruvost, F. Theodoro, A.L. Nguyen, S. Specklin, D. Kereselidze, C. Denis, B. Jego, P. Barbe, M. Keck, T. D'Anfray, B. Kuhnast, D. Audisio, C. Truillet, F. Taran, Chem. Sci. 15 (2024) 18825–18831.
[21] C.J. Yang, S.S. Ji, S. Shen, H.L. Yu, C.H. Deng, TrAC Trends Anal. Chem. 186 (2025) 118190.
[22] Y.L. Liu, S.Z. Yang, S.X. Li, Y.N. Wang, X.H. Liu, W. Xu, H.Y. Su, K. Qian, Small 21 (2025) 2409714.
[23] R.N. Ma, M.H. Lu, L. Ding, H.X. Ju, Z.W. Cai, Chem. Eur. J. 19 (2013) 102–108.
[24] H. He, Z.C. Guo, Y.R. Wen, S.X. Xu, Z. Liu, Anal. Chim. Acta 1090 (2019) 1–22.
[25] W. Ma, S.T. Xu, H.G. Nie, B.Y. Hu, Y. Bai, H.W. Liu, Chem. Sci. 10 (2019) 2320–2325.
[26] Y.L. Wang, Y.Y. Cui, Y.L. Zhao, R. Liu, Z.P. Sun, W. Li, X.Y. Gao, Chem. Commun. 48 (2012) 871–873.
[27] Y. Sun, W.H. Xie, F.Y. Shi, J.C. Li, H.X. Yu, Y.J. Jiang, C.H. Deng, Y.H. Deng, Adv. Mater. 38 (2025) e13988.
[28] N. Shalkevich, W. Escher, T. Burgi, B. Michel, L. Si-Ahmed, D. Poulikakos, Langmuir 26 (2010) 663–670.
[29] H. Kawasaki, T. Sugitani, T. Watanabe, T. Yonezawa, H. Moriwaki, R. Arakawa, Anal. Chem. 80 (2008) 7524–7533.
[30] Z.J. Zhu, P.S. Ghosh, O.R. Miranda, R.W. Vachet, V.M. Rotello, J. Am. Chem. Soc. 130 (2008) 14139–14143.
[31] P. Pomastowski, B. Buszewski, Nanomaterials 9 (2019) 260.
[32] J.T. Zhai, Y.L. Wang, J.X. Lu, C.N. Chen, J.Q. Liu, H.K. Zhao, N. Lu, Sens. Actuators B Chem. 409 (2024) 135560.
[33] M.N. Luo, L. Hou, J. Li, S. Shao, S.K. Huang, D. Meng, L.F. Liu, L. Feng, P. Xia, T. J. Qin, X.H. Zhao, Cancer Lett. 373 (2016) 1–11.
[34] F.N. Zhang, S.P. Wang, L.L. Yin, Y.Z. Yang, Y. Guan, W. Wang, H. Xu, N.J. Tao, Anal. Chem. 87 (2015) 9960–9965.
[35] B.C. Liu, D.M. Han, T.T. Zhang, G.H. Cheng, Y.L. Lu, J.B. Wang, H.F. Zhao, Z. P. Zhao, Int. J. Biochem. Cell. Biol. 111 (2019) 12–18.
[36] J.Y. Zhang, X.S. Zhang, Z.Y. Li, Q.S. Wang, Y. Shi, X. Jiang, X.Y. Sun, Front. Oncol. 11 (2021) 654672.
[37] P. Sharma, S. Hu-Lieskovan, J.A. Wargo, A. Ribas, Cell 168 (2017) 707–723.
[38] Y.L. Xie, J.W. Ding, X.L. Cui, M. Wu, C.C. Huang, R.Y. Zhang, J. Wang, X.Y. Li, S. Cen, J.M. Zhou, Eur. J. Pharm. Sci. 142 (2020) 105088.
[39] I.M. Bachmann, R.G. Ladstein, O. Straume, G.N. Naumov, L.A. Akslen, BMC Cancer 8 (2008) 362.
[40] A.A. Changavi, A. Shashikala, A.S. Ramji, J. Lab. Physicians 7 (2015) 079–083.
[41] A. Casazza, X. Fu, I. Johansson, L. Capparuccia, F. Andersson, A. Giustacchini, M. L. Squadrito, M.A. Venneri, M. Mazzone, E. Larsson, P. Carmeliet, M. De Palma, L. Naldini, L. Tamagnone, C. Rolny, Arterioscler. Thromb. Vasc. Biol. 31 (2011) 741–749.
[42] M. Warny, C.P. Kelly, Am. J. Physiol. Cell Physiol. 276 (1999) 717–724.
[43] J. Lim, S. Lee, Y.S. Hong, J.H. Choi, A. Jo, J.L. Kang, T.J. Song, Y.H. Choi, Int. J. Mol. Sci. 27 (2026) 474.
[44] Y.Y. Wu, Y.L. Chen, Y.C. Jao, I.S. Hsieh, K.C. Chang, T.M. Hong, Angiogenesis 17 (2014) 247–260.
[45] R. Max, R.R.C.M. Gerritsen, P.T.G.A. Nooijen, S.L. Goodman, A. Sutter, U. Keilholz, D.J. Ruiter, R.M.W. De Waal, Int. J. Cancer 71 (1997) 320–324.
[46] W.S. Moon, H.S. Park, K.H. Yu, M.Y. Park, K.R. Kim, K.Y. Jang, J.S. Kim, B.H. Cho, Hum. Pathol. 37 (2006) 1324–1332.

Jiahui Sun is pursuing her Ph.D. in analytical chemistry at Nanjing University. Her research interests include multiplex detection and imaging of biomarkers using functional mass nanoprobes.

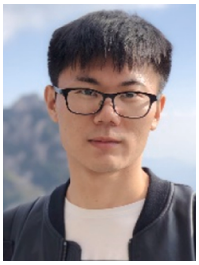

Dr. Nan Feng received his B.S. degree in 2016 and Ph.D. degree in 2023 from Nanjing University. Now he is an engineer in Southeast University. His research focuses on mass spectrometric biosensing and imaging.

Si Zhang received her master's degree in chemistry from Henan University. She is a Ph.D. candidate in Prof. Huangxian Ju's group at Nanjing University. Her research interests mainly focuses on structural analysis, nanoprobes and biosensing.

Mengchen Wang received her master's degree in chemistry from Nanjing University in 2025. Her research is focusing on utilizing series of mass nanoprobes with nucleic acids and antibodies to investigate the protein expression and protein dimerization. Her work aims to detect multiplexed proteins associated with diseases.

Huangxian Ju received his BS, MS and Ph.D. degrees from Nanjing University during 1982–1992. He is currently the director of the State Key Laboratory of Analytical Chemistry for Life Science, a Chief Scientist of the National Key Basic Research Program ('973 Program'), an Awardee of the National Science Fund for Distinguished Young Scholars, Chang Jiang Scholars Program and the 2022 Advances in Measurement Science Lectureship Award. His research focus on nanobiosensing, analytical biochemistry and molecular diagnosis. He has published 1010 papers in different journals with Google Scholar h-index 124 and more than 60200 citations.